JOURNAL OF QUATERNARY SCIENCE (2004) **19**(8) 763–768

Published online 29 September 2004 in Wiley InterScience (www.interscience.wiley.com). DOI: 10.1002/jqs.875

Towards automation of palynology 3: pollen pattern recognition using Gabor transforms and digital moments

Y. ZHANG,[1]* D. W. FOUNTAIN,[1] R. M. HODGSON,[2] J. R. FLENLEY[3] and S. GUNETILEKE[2]
[1] Institute of Molecular BioSciences, Massey University, Palmerston North, New Zealand
[2] Institute of Information Sciences and Technology, Massey University, Palmerston North, New Zealand
[3] School of People, Environment and Planning, Massey University, Palmerston North, New Zealand

Zhang, Y., Fountain, D. W., Hodgson, R. M., Flenley, J. R. and Gunetileke, S. 2004. Towards automation of palynology 3: pollen pattern recognition using Gabor transforms and digital moments. *J. Quaternary Sci.*, **Vol. 19** pp. 763–768. ISSN 0267-8179.

Received 3 January 2003; Revised 25 July 2003; Accepted 1 July 2004

ABSTRACT: The classification of pollen grains using texture information in combination with shape features is presented in this paper. The surface texture of pollen is characterised by using Gabor transforms, the geometric shape is described by using moment invariants, and the pollen grains are classified by an artificial neural network. In an experiment with five types of pollen grains, more than 97% of samples are correctly classified. Copyright © 2004 John Wiley & Sons, Ltd.

KEYWORDS: pollen analysis; Gabor transforms; moment invariants; neural network.

JQS
Journal of Quaternary Science

Introduction

Distinguishing plant species through analysis of their pollen grains is widely used for palaeoenvironmental reconstruction, inferring the geological past, and in medical studies. The connection between some types of asthma and inhalant allergic reactions and pollen in the atmosphere has long been established (Taylor *et al.*, 2000; Fountain, 2002). The assessment of the types and abundance of allergenic pollen in the atmosphere has been an essential underpinning for such studies. Well-developed pollen-counting networks exist in several countries. In Europe, 25 countries (with 400 stations) contribute to the European Aeroallergen Network (EAN). In the USA the National Allergy Bureau provides pollen counts from 65 air sampling stations in all states. Each counting station is certified—a training programme is required, and most are volunteer-manned. Other countries with histories of pollen and spore counting are Canada, Mexico, Australia and countries of South America. However, pollen analysis is time-consuming, laborious and highly skilled work.

The development of an automated system for identifying pollen grains has considerable significance for all the above fields, especially for better establishing the relationship of particular pollens to allergy and asthma. The advantages that would arise if such a system could be developed have been recently summarised (Stillman and Flenley, 1996). The application of image processing and pattern recognition techniques is a key to developing such a system. Some statistical and neural network techniques have been studied for identification of surface textures of pollen grains (Treloar, 1992; Li and Flenley, 1999; Langford *et al.*, 1990).

In the past, two kinds of microscopic images have been used to perform pollen analysis; one is scanning electron microscope (SEM) images, the other is light microscope (LM) images. The former is expensive and difficult to produce for a mixed pollen assemblage. The present work uses light microscope images as a basis.

For the way towards the important goal of automating the identification of pollen based on LM images, a method of pollen image description is proposed based on texture information in combination with shape features, in which Gabor wavelet transform is employed to describe surface textures, and moment invariants based on region are used to measure the shape.

To recognise pollen images, the multilayer perceptron (MLP) neural network is adopted by using Gabor wavelet features and moment invariants as the inputs, and the neural network is trained by a back-propagation algorithm.

Pollen image acquisitions and pre-processing

In this research a system as shown in Fig. 1 is used to perform pollen analysis. The slides with pollen particles are first

* Correspondence to: Yongping Zhang, The Institute of Molecular BioSciences, Massey University, Private Bag 11 222, Palmerston North, New Zealand.
E-mail: Zhangyp1963@yahoo.com

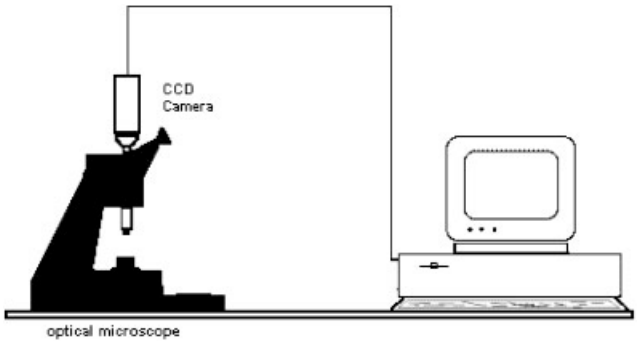

Figure 1 The system of image capture

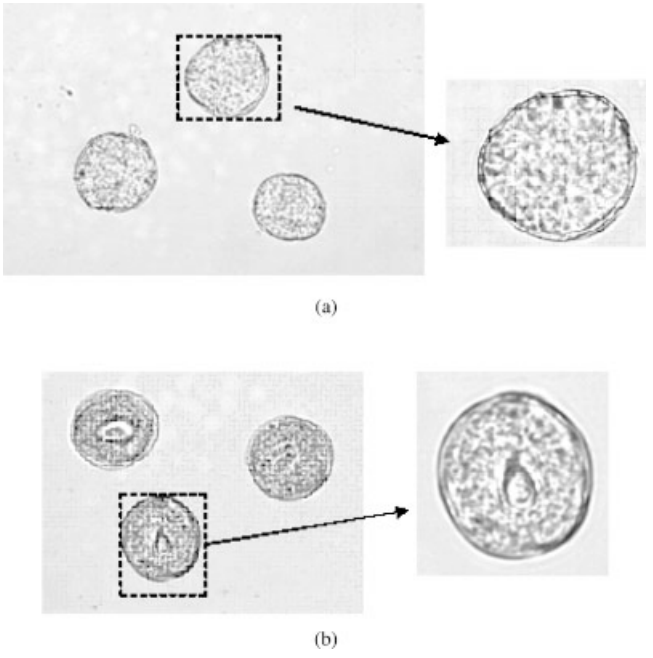

Figure 2 Image illustrating *Delphinium* pollen in slide preparations: (a) unstained pollen; (b) stained pollen

prepared for microscopy. Each slide is stained with Calberla's solution (Basic Fuchsin stain), and then, under the optical microscope, the mid-equatorial surface images of pollen grains are captured by CCD camera at $\times 400$ magnification.

Stained and unstained pollen grains for the same type of pollen are quite different in textural appearance under microscopy. As an example, we use non-airborne fresh pollen of *Delphinium*. Figure 2 shows a representative image illustrating fresh *Delphinium* pollen in slide preparations. Figure 2(a) shows an unstained grain and in Fig. 2(b) a stained grain is presented. For different cases, the image illustrations appear to be quite different. The results indicate that the slide preparation is also important for automatic pollen discrimination. For consistency, all the pollen grains used in this paper were stained.

Materials

The taxa used in this study are five New Zealand modern pollen types: *Bidens pilosa* (BP; Fig. 3(a)), *Cyathea medullaris* (CM; Fig. 3(b)), *Hypochoeris radicata* (HR; Fig. 3(c)), *Passiflora quadrangularis* (PQ; Fig. 3(d)) and *Pseudelephantopus spicatus* (PS; Fig. 3(e)). The corresponding sampled texture images for each surface image presented in Fig. 3 are shown in Fig. 4. For each type of pollen grains, 18 texture samples were used in this research. The collection of all the samples for five types of pollen grains is shown in Fig. 5.

Image enhancement

For the images captured, we used a 3×3 median filter to reduce random noise. Since we were interested in texture and shape in the surface of pollen grains, pollen segmentation was done. All segmented images were adjusted by using a high-emphasis filter (or shadow correction) (Narendra, 1981) to enhance the details of images. The high-emphasis filter we used is:

$$\begin{aligned} H_{\text{high-emphasis}} &= \alpha \cdot H_{\text{high-pass}} + H_{\text{low-pass}} \\ &= \alpha \cdot (1 - H_{\text{low-pass}}) + H_{\text{low-pass}} \end{aligned} \quad (1)$$

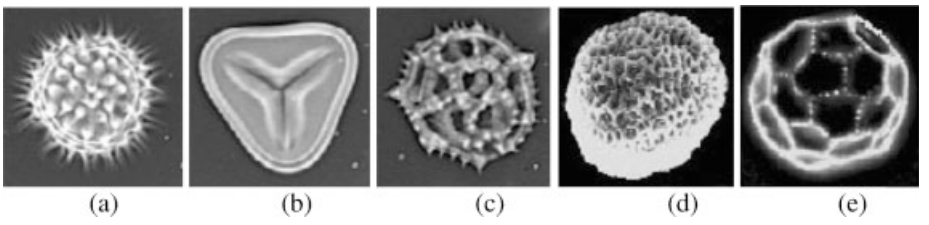

Figure 3 Pollen surface images. (a) *Bidens pilosa* (BP). (b) *Cythea medullaris* (CM). (c) *Hypochoeris radicata* (HR). (d) *Passiflora quadrangularis* (PQ). (e) *Pseudelephantopus spicatus* (PS)

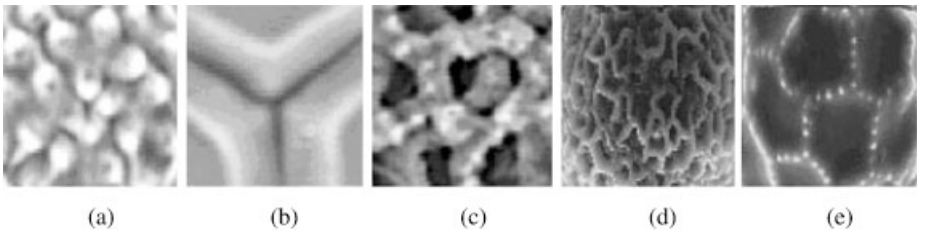

Figure 4 Texture samples. (a) Typical texture of BP. (b) Typical texture of CM. (c) Typical texture of HR. (d) Typical texture of PQ. (e) Typical texture of PS

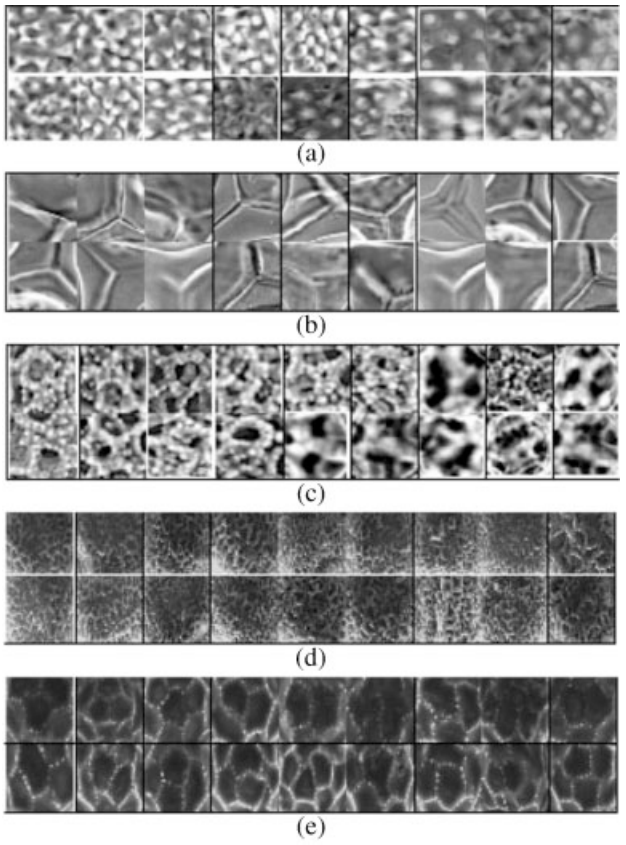

Figure 5 Texture images used in the experiment. From (a) to (e), samples of BP, samples of CM, samples of HR, samples of PQ and samples of PS

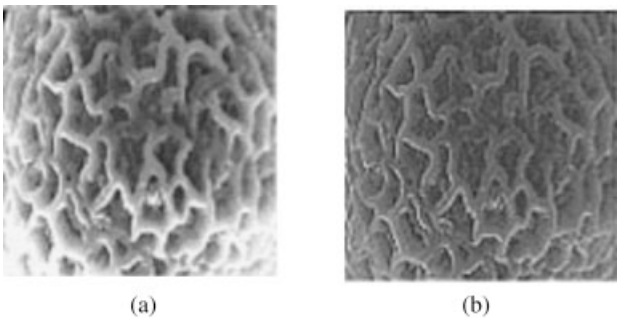

Figure 6 High-emphasis filtering: (a) the original images; (b) the intensity-adjusted image

where α is an adjustable constant. The parameter α controls the amplification of the high-frequency components. The low-pass filter $H_{\text{low-pass}}$ is Gaussian with 3×3 operations:

$$H_{\text{low-pass}} = \frac{1}{16}\begin{bmatrix} 1 & 2 & 1 \\ 2 & 4 & 2 \\ 1 & 2 & 1 \end{bmatrix}$$

For larger values of parameter α, the high-frequency will be overcompensated resulting in white bands being formed along the edges of objects. In order to avoid overcompensation of high-frequency information, a suitable parameter α must be chosen. In general, if the high-frequency components are blown up more than ten times ($\alpha = 10$), the overcompensation will happen. Here we propose an adaptive method for selection of parameters based on information entropy. For a given image $I(x, y)$ and a parameter α, the output image $I_\alpha(x, y)$ of

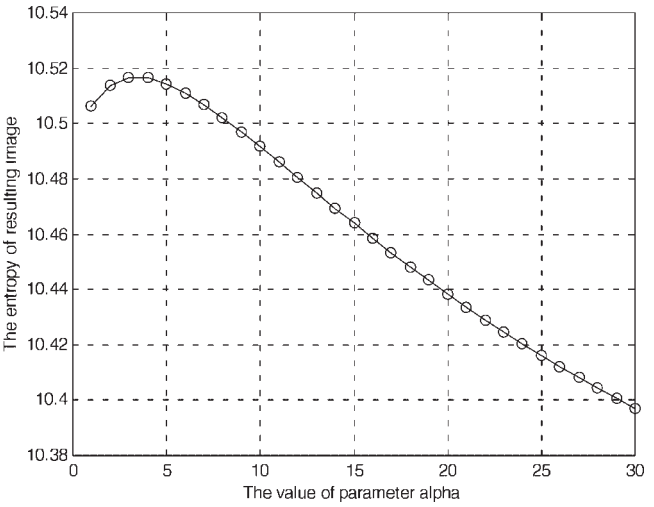

Figure 7 The entropy variation curve for filtering outputs of Fig. 3(a)

filtering is first normalised to $\bar{I}_\alpha(x, y)$ with mean value 1, and the entropy is then defined as:

$$ENT_\alpha = -\sum_{x,y} \bar{I}_\alpha(x, y) \log[\bar{I}_\alpha(x, y)] \tag{2}$$

For the parameters of a certain range (here $\alpha \in N$, $1 \leq \alpha \leq 30$), the entropies are computed; and then the parameter corresponding to the maximum entropy is selected. Figure 6 shows an example of such processing, where the parameter α was chosen as 4 according to the entropy variation curve (Fig. 7).

Texture description

Gabor filtering techniques have been shown to have good performance in texture discrimination and segmentation (Daugman, 1980; Reed *et al.*, 1990; Antonie *et al.*, 1997; Fayolle *et al.*, 1998, 2000; Tieng and Boles, 1997; Khalil and Bayoumi, 1999). In this section, a method of texture presentation is introduced based on Gabor wavelet transforms.

Gabor filter

2-D Gabor elementary function is Gaussian modulated by a complex sinusoid which has the following form:

$$\begin{aligned} \Psi(x, y) &= \exp\left[-\frac{1}{8}(4x^2 + y^2)\right] \cdot \exp(\mathrm{i})\omega x \\ &= \exp\left[-\frac{1}{8}(4x^2 + y^2)\right] \cdot \cos(\omega x) \\ &\quad + \mathrm{i} \cdot \exp\left[-\frac{1}{8}(4x^2 + y^2)\right] \cdot \sin(\omega x) \end{aligned} \tag{3}$$

where ω is the radial frequency of the filter. By scale dilation and orientation rotation, a family of filters is obtained as the follows:

$$\begin{aligned} \Psi_{m,n}(x, y) = \alpha_0^{-m} \exp\Bigg\{ &-\frac{\alpha_0^{-2m}}{8}\left[4\left(x\cos\frac{n\pi}{K} + y\sin\frac{n\pi}{K}\right)^2\right. \\ &\left.+\left(-x\sin\frac{n\pi}{K} + y\cos\frac{n\pi}{K}\right)^2\right]\Bigg\} \\ &\times \exp\left[\mathrm{i}\omega\omega_0^{-m}\left(x\cos\frac{n\pi}{K} + y\sin\frac{n\pi}{K}\right)\right] \end{aligned} \tag{4}$$

where K is the total number of orientations, $\alpha_0 > 0$, $m, n \in \mathrm{N} \cup \{0\}$ and $n < K$.

The real and the imaginary parts of the filter (3) are the so-called even- and odd-symmetric filters respectively. Both them are usually used together or independently to represent texture. For a given image $I(x, y)$, if we denote by $W_{m,n}(x, y)$ and $W^*(x, y)$ the responses of the Gabor filter and the conjugate Gabor filter respectively, the following real wavelet transform is just the response of the even-symmetric filter $\overline{\Psi}(x, y)$:

$$\begin{aligned}\overline{W}_{m,n}(x, y) &= \frac{1}{2}\left[W_{m,n}(x, y) + W^*_{m,n}(x, y)\right] \\ &= \int\int I(s, t)\overline{\Psi}_{m,n}(x - s, y - t)\,\mathrm{d}s\,\mathrm{d}t\end{aligned} \tag{5}$$

The even-symmetric Gabor filters have been shown to be effective for pre-attentive (attention to global feature) texture discrimination (Malik and Perona, 1990). Here the even-symmetric Gabor filter is selected; this filter $\overline{\Psi}(x, y)$ is as follows:

$$\overline{\Psi}(x, y) = \exp\left[-\frac{1}{8}(4x^2 + y^2)\right] \cdot \cos(\omega x) \tag{6}$$

Similarly, a family of filters as in (4) can be derived from filter $\overline{\Psi}(x, y)$. For a given image $I(x, y)$ and each pair (m, n), we denote the corresponding output as $\overline{W}_{m,n}(x, y)$ $(m, n \in \mathrm{N} \cup \{0\}$ and $n < K)$.

In order to form rotational invariant texture features, we use the average of Gabor transforms corresponding to different directions to describe the local structures for a given image $I(x, y)$:

$$Gf_m(x, y) = \frac{1}{K}\sum_{n=0}^{K-1}\overline{W}_{m,n}(x, y) \tag{7}$$

The mean value (μ_m) and standard deviation (σ_m) of $Gf_m(x, y)$ are chosen to represent texture features. Thus, a $2S$-dimensional feature vector, $\bar{\nu} = (\mu_0, \sigma_0, \mu_1, \sigma_1, \ldots, \mu_{S-1}, \sigma_{S-1})$, is extracted from the given image.

Filter design

The spatial frequency responses of the Gabor functions are central symmetry in the frequency domain; only half the frequency plane is needed for texture description (Daugman, 1980; Reed *et al.*, 1990). In this study, six values of orientation are used, i.e. the parameter K is chosen as 6, so that $n = 0, 1, 2, 3, 4, 5$. The values of a_0^{-m} present the window sizes of filters; in general these should be chosen to not be beyond the quarter of either the width or height of the input image. In the dyadic way, the parameter a_0 is fixed as $1/\sqrt{2}$, and the parameter m should be chosen as no more than 8 because the texture samples used in our experiment have the average size 64×64. In this study, the values of parameter m are chosen as 0, 1, 2, 3, 4, 5, 6, 7, 8, i.e. $S = 9$.

For the fixed scale parameter m, we let $\vec{f}_m = (\mu_m, \sigma_m)$. The scatter diagrams of Gabor features corresponding to three different scale parameters for the 90 (18×5) images are plotted in Fig. 8.

For the purpose of feature selection, we use the interclass/intraclass distance to measure the discrimination performance of the individual feature vector $\vec{f} = (\mu, \sigma)$ corresponding to a different scale. This measurement is defined as:

$$J = \frac{\sum_{k=1}^{C} N_k \left\|\vec{\Pi}_k - \vec{\Pi}\right\|^2}{\sum_{k=1}^{C}\sum_{n=1}^{N_k}\left\|\vec{f}_{k,n} - \vec{\Pi}_k\right\|^2} \tag{8}$$

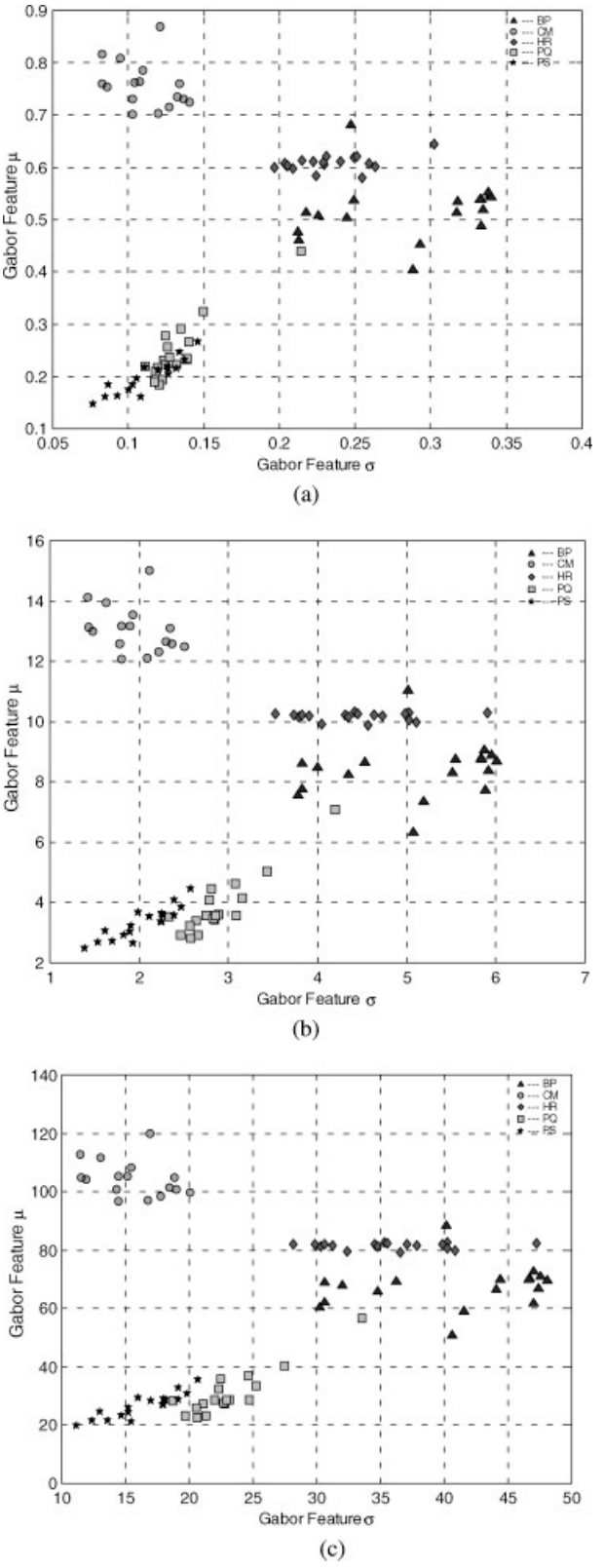

Figure 8 The scatter diagrams for Gabor features of pollen texture images corresponding to different scales. (a) Scale parameter $m = 1$. (b) Scale parameter $m = 4$. (c) Scale parameter $m = 6$

where $\vec{f}_{k,n}$ is the feature vectors of the nth pattern in the kth class, C is the number of classes, N_k is the number of samples in the kth class, $\vec{\Pi}_k$ is the mean of feature vectors for all the samples in the kth class, $\vec{\Pi}$ is the mean of feature vectors for all the samples in the entire training set, and $\|\cdot\|$ is Euclidean distance. By computing for a smaller scale, the discrimination

performance is better, and the parameter m greater than 6 can be accepted. The fact is also reflected by Fig. 8. This indicates that higher frequency components have a better discrimination.

Moment invariants

Based on the histogram of grey-level, a binarization process is implemented for the input image. If we denote by R the region (whose shape we want to describe) of points so that $I_p(x, y) = 1$, then the digital i, jth moment of R is defined by:

$$M_{ij}(R) = \sum_{(x,y)\in R} x^i y^j \tag{9}$$

M_{00} is the number of points in the region R and represents the area of R. The centroid of R is expressed as:

$$(\bar{x}, \bar{y}) = (M_{10}/M_{00}, M_{01}/M_{00}) \tag{10}$$

The central I, jth moments are defined by:

$$m_{ij}(R) = \sum_{(x,y)\in R} (x - \bar{x})^i (y - \bar{y})^j \tag{11}$$

A set of parameters can be then derived from the previous eight central moments. In general, from the central moments up to order three, seven parameters are extracted and used as shape descriptors. These are invariant under translation, rotation and scaling, hence they are called moment invariants (Hu, 1962). There are two second-order moment invariants which are defined by:

$$M_1 = (m_{20} + m_{02})/m_{00}^2, \quad M_2 = \left[(m_{20} - m_{02})^2 + 4m_{11}^2\right]/m_{00}^2 \tag{12}$$

The multilayer perceptron classifier

Neural networks can be used to solve both supervised and unsupervised classification/recognition problems (Pandya and Macy, 1996). In the present study, we use a MLP neural network with a single hidden layer as classifier to identify the feature vectors of pollen patterns.

For each image, two second-order central moments and four Gabor features corresponding to two scales are extracted, and then a six-dimensional feature vector is formed. We select the number of input nodes of MLP to be six, which is equal to the dimension of feature vectors. The number of output nodes is equal to the number of training models (here it is five). Based on Kolmogorov theory, for a neural network with N input nodes, the number of the hidden nodes should be $2N + 1$ (Annema, 1995; Hecht-Nielsen, 1987, 1989). Here we choose the number of nodes in the hidden layer to be 13 ($2 \times 6 + 1$). The architecture of this neural network is shown in Fig. 9. Such a network can be shown mathematically as:

$$out_i = \varphi\left(\sum_j w_{ij} out_j + \theta_i\right) \tag{13}$$

where out_i is the output of the ith node in the layer under consideration; out_j is the output of the jth node in the preceding layer. The nonlinear activation function φ is a sigmoid function, i.e. $\phi(t) = 1/(1 + e^{-t})$. For training the neural network, the back-propagation algorithm (Pandya and Macy, 1996) is utilised.

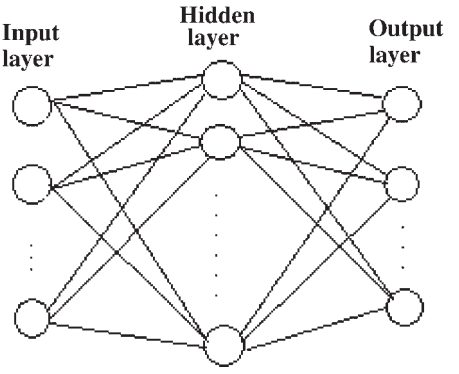

Figure 9 Fully connected multilayer perceptron neural network with one hidden layer. There are six nodes in the input layer, 13 nodes in the hidden layer and five nodes in the output layer

Experimental results

Here five types of pollen grains, as shown in Fig. 3, have been examined. Training and testing samples are generated by rotating each sampled image (shown in Fig. 5) by three different orientations (here 45°, 90°, 135°). Half of them are used for training; the remaining half are used for testing. Thus 36 texture images for each type of pollen grain need to be identified. In the experiment, the scale parameter m is selected as 7, 8. The inputs of the neural network are six-dimensional feature vectors, i.e. two components are moment invariants and four components are Gabor features. The components of these vectors are arranged as (M_1, M_2, μ_7, σ_7, μ_8, σ_8). The classification results with texture images are summarised in Table 1. In this experiment, 97.7% of texture images are correctly classified.

Conclusions

This paper has proposed a recognition system which is based on texture information in combination with shape features to recognise pollen grains. The Gabor features corresponding to different scales and the moment invariants based on region are computed. The identification is done by a feedforward neural network trained by the back-propagation algorithm. In the experiment with five pollen types, more than 97% of texture images are correctly identified.

Table 1 Classification results

Desired class \ Class matched	BP	CM	HR	PQ	PS
BP	32	0	3	0	1
CM	0	36	0	0	0
HR	0	1	35	0	0
PQ	0	0	0	36	0
PS	0	0	0	0	36

References

Annema AJ. 1995. *Feed-Forward Neural Network: Vector Decomposition Analysis Modeling and Analog Implementation*. Kluwer: New York.

Antonie JP, Barache D, Cesar RM, da Fontoura Costa L. 1997. Shape characterization with the wavelet transform. *Signal Processing* **62**: 265–290.

Daugman JG. 1980. Two-dimensional spectral analysis of cortical receptive field profiles. *Vision Research* **20**: 847–856.

Fayolle J, Ducottet C, Schon JP. 1998. Application of multiscale characterization of edges to motion determination. *IEEE Transactions on Signal Processing* **46**(4): 1174–1179.

Fayolle J, Riou L, Ducottet C. 2000. Robustness of a multiscale scheme of feature points detection. *Pattern Recognition* **33**(9): 1437–1453.

Fountain DW. 2002. Pollen and inhalant allergy. *Biologist* **49**(1): 5–9.

Hecht-Nielsen R. 1987. Kolmogorov's mapping neural networks existence theorem. *Proceedings of the First IEEE International Conference on Neural Networks*, Vol. 3. San Diego, CA: 112–114.

Hecht-Nielsen R. 1989. Theory of backpropagation neural networks. *Proceedings of the International Joint Conference on Neural Networks*, Vol. 1. Washington, DC: 593–605.

Hu MK. 1962. Visual pattern recognition by moment invariants. *IRE Transactions on Information Theory* **IT-8**: 179–187.

Khalil MI, Bayoumi MM. 1999. Invariant 2D object recognition using the wavelet transform and structured neural networks. In *AeroSence'99, SPIE Conference on Wavelet Applications*, VI. Orlando, FL: 330–340.

Langford M, Taylor GE, Flenley JR. 1990. Computerised identification of pollen grains by texture analysis. *Review of Palaeobotany and Palynology* **64**: 197–203.

Li P, Flenley JR. 1999. Pollen texture identification using neural networks. *Grana* **38**: 59–64.

Malik J, Perona P. 1990. Preattentive texture discrimination with early vision mechanisms. *Journal of the Optical Society of America A: Optics and Image Science* **7**(5): 923–932.

Narendra PM, Fitch RC. 1981. Real-time adaptive contrast enhancement. *IEEE Transactions on Pattern Analysis and Machine Intelligence* **3**(6): 655–661.

Pandya AS, Macy RB. 1996. *Pattern Recognition with Neural Networks in C++*. CRC and IEEE Press: Boca Raton, FL.

Reed TR, Wechsler H. 1990. Segmentation of textured images and Gestalt organization using spatial/spatial-frequency representations. *IEEE Transactions on Pattern Analysis and Machine Intelligence* **PAMI-12**: 1–12.

Stillman EC, Flenley JR. 1996. The needs and prospects for automation in palynology. *Quaternary Science Reviews* **15**: 15.

Taylor PE, Flagan RC, Valenta R, Glovsky MM. 2002. Release of allergens as respirable aerosols: a link between grass pollen and asthma. *Journal of Allergy and Clinical Immunology* **109**: 51–55.

Tieng QM, Boles WW. 1997. Recognition of 2D object contours using the wavelet transform zero-crossing representation. *IEEE Transactions on Pattern Analysis and Machine Intelligence* **19**(8): 910–916.

Treloar WJ. 1992. Digital image processing techniques and their application to the automation of palynology. *PhD thesis*, University of Hull.